Nuclear mean field and double-folding model of the nucleus-nucleus optical potential

Dao T. Khoa,[1,*] Nguyen Hoang Phuc,[1] Doan Thi Loan,[1] and Bui Minh Loc[1,2]

[1]*Institute for Nuclear Science and Technology, VINATOM, 179 Hoang Quoc Viet, Cau Giay, Hanoi, Vietnam*
[2]*University of Pedagogy, Ho Chi Minh City, Vietnam*

Realistic density dependent CDM3Yn versions of the M3Y interaction have been used in an extended Hartree-Fock (HF) calculation of nuclear matter (NM), with the nucleon single-particle potential determined from the total NM energy based on the Hugenholtz–van Hove theorem that gives rise naturally to a rearrangement term (RT). Using the RT of the single-nucleon potential obtained exactly at different NM densities, the density and energy dependence of the CDM3Yn interactions was modified to account properly for both the RT and observed energy dependence of the nucleon optical potential. Based on a local density approximation, the double-folding model of the nucleus-nucleus optical potential has been extended to take into account consistently the rearrangement effect and energy dependence of the nuclear mean-field potential, using the modified CDM3Yn interactions. The extended double-folding model was applied to study the elastic $^{12}\text{C}+^{12}\text{C}$ and $^{16}\text{O}+^{12}\text{C}$ scattering at the refractive energies, where the Airy structure of the nuclear rainbow has been well established. The RT was found to affect significantly the real nucleus-nucleus optical potential at small internuclear distances, giving a potential strength close to that implied by the realistic optical model description of the Airy oscillation.

I. INTRODUCTION

During the last three decades, the double-folding model (DFM) of the nucleus-nucleus optical potential (see, e.g., Refs. [1–5] and references therein) has been successfully used to calculate the real heavy-ion (HI) optical potential (OP) for use in different nuclear reaction studies. It is straightforward to see from the basic folding formulas that the folding model generates the first-order (Hartree-Fock type) term of Feshbach's microscopic OP [6]. The success of the folding model description the observed elastic scattering of numerous HI systems, in particular, the nuclear rainbow pattern observed in the elastic scattering of the light HI systems [7], clearly suggests that the first-order term of Feshbach's microscopic OP is indeed the dominant part of the real nucleus-nucleus OP.

The basic inputs for a folding model calculation are the nuclear densities of the colliding nuclei and the effective nucleon-nucleon (NN) interaction between the projectile nucleons and those in the target. A popular choice in the past for the effective NN interaction has been the M3Y interaction [1], which was designed to reproduce the G-matrix elements of the Reid [8] and Paris [9] NN potentials in an oscillator basis. The original (density independent) M3Y interaction was used with some success in the folding model calculation of the real HI optical potential at low energies [1], where the elastic scattering data are sensitive to the potential only at the surface, near the strong absorption radius $R_{\text{s.a.}}$. The situation becomes different in cases of the refractive nucleus-nucleus scattering with the observation of the nuclear rainbow pattern [5], where the elastic data measured at large angles were shown to be sensitive to the real OP over a wider radial range, down to small distances $R < R_{\text{s.a.}}$. Here, the original M3Y interaction failed to give a good description of the data, and several realistic

choices of the density dependence were included in the M3Y interaction [2,3,5,10,11] to account for the reduction of the *attractive* strength of the effective NN interaction at high densities of the nuclear medium, as the two nuclei closely approach and overlap with each other at small distances.

The explicit density dependence of the M3Y interaction considered in the present work was parametrized [2,3,11] to reproduce the saturation properties of symmetric nuclear matter (NM) in the standard Hartree-Fock (HF) calculation. To have a reliable density dependent interaction for use at different energies, the nucleon OP in NM obtained in the HF calculation [11,12] (or the high-momentum part of the HF single-nucleon potential) was used to adjust the explicit energy dependence of the density dependent M3Y interaction against the observed energy dependence of the nucleon OP. However, the HF single-nucleon potential [11,12] is roughly equivalent to the single-particle potential of the Brueckner-Bethe theory [13], which lacks the *rearrangement* term that arises naturally in the Landau theory for infinite Fermi systems [14]. Such a rearrangement term (RT) also appears when the single-nucleon potential is evaluated from the total NM energy using the Hugenholtz and van Hove (HvH) theorem [15], which is exact for all systems of interacting fermions, independent of the type of the interaction between fermions.

For infinite NM, it is straightforward to see that the HvH theorem is satisfied on the HF level only when the in-medium NN interaction is density independent, i.e., when the RT is equal zero [16]. As a result, the single-nucleon (or nucleon mean-field) potential in NM evaluated on the HF level using an in-medium, density dependent NN interaction is not compliant with the HvH theorem. It is of interest, therefore, to have a method to take into account properly the RT of the single-nucleon potential in NM on the HF level using the same density dependent NN interaction that was determined to reproduce the saturation properties of symmetric NM. Based on the exact expression of the RT of the single-nucleon potential given by

*khoa@vinatom.gov.vn

the HvH theorem at each NM density and the empirical energy dependence of the nucleon OP observed over a wide range of energies, a compact method has been suggested recently [17] to account effectively for the RT in the standard HF scheme, by supplementing the density dependent CDM3Yn interaction [3] with the explicit contributions of the RT and of the momentum dependence of the nucleon mean-field potential.

For finite nuclei, the RT appears naturally [18,19] when the variational principle is applied to solve the eigenvalue problem in the HF calculation, using an effective density dependent NN interaction. Such a RT in the HF energy density of finite nuclei is known to describe the rearrangement of the mean field due to the removal or addition of a single particle [20]. In fact, it has been observed experimentally in the nucleon removal reactions at low energies that the interaction between the projectile nucleon and a target nucleon can induce some rearrangement of the single-particle configurations of other nucleons in the target [21]. In terms of the nucleus-nucleus interaction, such a rearrangement effect should also affect the shape and strength of the microscopic nucleus-nucleus OP constructed in the folding model using the single-particle wave functions of the projectile- and target nucleons. Because the standard double-folding calculations of the nucleus-nucleus potential are being done mainly on the HF level [3–5], the impact of the rearrangement effect to the folded nucleus-nucleus OP has not been studied so far.

The present work is the first attempt to address this important issue. For this purpose, an extended version of the DFM is proposed to effectively include the RT into the folded nucleus-nucleus OP in the same mean-field manner, using consistently the same density and momentum dependent CDM3Yn interaction determined from the extended HF study of NM [17] to be compliant with the HvH theorem. The extended DFM is applied to study in detail the impact of the rearrangement effect of the nuclear mean field in the optical model analysis of the elastic, refractive ^{12}C $+^{12}$C and ^{16}O $+^{12}$C scattering at different energies.

II. SINGLE-NUCLEON POTENTIAL IN THE EXTENDED HF FORMALISM

We recall here the (nonrelativistic) Hartree-Fock description of homogeneous and symmetric NM at the given nucleon density ρ. Given the direct (v_c^D) and exchange (v_c^{EX}) parts of the (central) effective NN interaction v_c, the ground-state energy of NM is $E = E_{kin} + E_{pot}$, where the kinetic and potential energies are determined as

$$E_{kin}(\rho) = \sum_{k\sigma\tau} n(k)\frac{\hbar^2 k^2}{2m_\tau} \quad (1)$$

$$\begin{aligned} E_{pot}(\rho) &= \frac{1}{2}\sum_{k\sigma\tau}\sum_{k'\sigma'\tau'} n(k)n(k')[\langle k\sigma\tau,k'\sigma'\tau'|v_c^D|k\sigma\tau,k'\sigma'\tau'\rangle \\ &\quad + \langle k\sigma\tau,k'\sigma'\tau'|v_c^{EX}|k'\sigma\tau,k\sigma'\tau'\rangle] \\ &= \frac{1}{2}\sum_{k\sigma\tau}\sum_{k'\sigma'\tau'} n(k)n(k')\langle k\sigma\tau,k'\sigma'\tau'|v_c|k\sigma\tau,k'\sigma'\tau'\rangle_{\mathcal{A}}. \end{aligned} \quad (2)$$

Here the single-particle wave function $|k\sigma\tau\rangle$ is plane wave. The nucleon momentum distribution $n(k)$ in the spin-saturated, symmetric NM is a step function determined with the Fermi momentum $k_F = (1.5\pi^2\rho)^{1/3}$ as

$$n(k) = \begin{cases} 1 & \text{if } k \leqslant k_F, \\ 0 & \text{otherwise.} \end{cases} \quad (3)$$

According to the Landau theory for infinite Fermi systems [13,14], the single-particle energy $\varepsilon(\rho,k)$ at the given nucleon density ρ is determined as

$$\varepsilon(\rho,k) = \frac{\partial E}{\partial n(k)} = t(k) + U(\rho,k) = \frac{\hbar^2 k^2}{2m} + U(\rho,k), \quad (4)$$

which is the change of the NM energy caused by the removal or addition of a nucleon with the momentum k. The single-particle potential $U(\rho,k)$ consists of both the HF and rearrangement terms,

$$U(\rho,k) = U_{HF}(\rho,k) + U_{RT}(\rho,k), \quad (5)$$

where $U_{HF}(\rho,k) = \sum_{k'\sigma'\tau'} n(k')\langle k\sigma\tau,k'\sigma'\tau'|v_c|k\sigma\tau,k'\sigma'\tau'\rangle_{\mathcal{A}}$

$$\qquad\qquad (6)$$

and $U_{RT}(\rho,k) = \frac{1}{2}\sum_{k_1\sigma_1\tau_1}\sum_{k_2\sigma_2\tau_2} n(k_1)n(k_2)$

$$\times \langle k_1\sigma_1\tau_1,k_2\sigma_2\tau_2|\frac{\partial v_c}{\partial n(k)}|k_1\sigma_1\tau_1,k_2\sigma_2\tau_2\rangle_{\mathcal{A}}. \quad (7)$$

It is clear from Eqs. (4) and (7) that the RT accounts for the rearrangement of the nuclear mean field due to the removal or addition of a nucleon [20]. When the nucleon momentum approaches the Fermi momentum ($k \to k_F$), $\varepsilon(\rho,k_F)$ determined from Eqs. (4)–(7) is exactly the Fermi energy given by the Hugenholtz–van Hove theorem [15]. Using the transformation

$$\frac{\partial}{\partial n(k)}\bigg|_{k\to k_F} = \frac{\partial\rho}{\partial n(k_F)}\frac{\partial k_F}{\partial\rho}\frac{\partial}{\partial k_F} = \frac{1}{2\Omega}\frac{\pi^2}{k_F^2}\frac{\partial}{\partial k_F}, \quad (8)$$

where Ω is the volume of symmetric NM, the RT of the single-particle potential U at the Fermi momentum can be obtained as

$$\begin{aligned} U_{RT}(\rho,k = k_F) &= \frac{4\pi^2}{k_F^2}\frac{\Omega}{(2\pi)^6}\iint n(k_1)n(k_2) \\ &\quad \times \langle k_1 k_2|\frac{\partial v_c}{\partial k_F}|k_1 k_2\rangle_{\mathcal{A}} d^3k_1 d^3k_2. \end{aligned} \quad (9)$$

In difference from the RT part, the HF part of the single-particle potential is readily evaluated at any momentum

$$U_{HF}(\rho,k) = \frac{4\Omega}{(2\pi)^3}\int n(k')\langle kk|v_c|kk'\rangle_{\mathcal{A}} d^3k'. \quad (10)$$

For the spin-saturated symmetric NM, the spin and isospin components of plane waves are averaged out in the HF calculation of the single-particle potential, and only the spin and isospin independent terms of the central NN interaction are needed for the determination of the single-particle potential (9)–(10). In the present work, we use two density dependent versions (CDM3Y3 and CDM3Y6) [3] of the M3Y interaction

based on the G-matrix elements of the Paris potential in an oscillator basis [9]. Thus, the central CDM3Yn interaction is determined explicitly as

$$v_c^{D(EX)}(s) = F_0(\rho)v_{00}^{D(EX)}(s), \quad \text{where } s = |\mathbf{r}_1 - \mathbf{r}_2|. \quad (11)$$

The radial part of the interaction $v_{00}^{D(EX)}(s)$ is kept unchanged as determined from the spin and isospin independent part of the M3Y-Paris interaction [9], in terms of three Yukawas:

$$v_{00}^D(s) = 11061.625\frac{\exp(-4s)}{4s} - 2537.5\frac{\exp(-2.5s)}{2.5s}$$
$$+ 0.0002\frac{\exp(-0.7072s)}{0.7072s},$$
$$v_{00}^{EX}(s) = -1524.25\frac{\exp(-4s)}{4s} - 518.75\frac{\exp(-2.5s)}{2.5s}$$
$$- 7.8474\frac{\exp(-0.7072s)}{0.7072s}.$$

The density dependence of the interaction (11) was assumed in Ref. [3] as a hybrid of the exponential and power-law forms in order to obtain different values of the nuclear incompressibility K in relatively small (10 to 20 MeV) steps from the HF calculation of NM. Given this empirical choice of $F_0(\rho)$, a realistic range for the K value (the most vital input for the equation of state of cold NM) has been deduced accurately from the folding model analysis of the refractive α-nucleus and nucleus-nucleus scattering (see details in the review [5]). Thus, we have used in the present work the following functional form for $F(\rho)$ [3]:

$$F_0(\rho) = C[1 + \alpha \exp(-\beta\rho) + \gamma\rho]. \quad (12)$$

Note that the interaction (11) is the *isoscalar* part of the central interaction. A more comprehensive HF study of the nucleon mean-field potential in asymmetric NM has been performed recently [17], taking into account also the isospin dependent part of the CDM3Yn interaction. In the DFM calculation of the nucleus-nucleus optical potential, the isospin dependent part of the effective NN interaction is needed only if both nuclei have nonzero isospins in their ground states [22]. In the present study we have focused, therefore, on the extension of the DFM using the spin and isospin independent interaction (11) only.

The parameters of the density dependence $F_0(\rho)$ were determined [3] to reproduce on the HF level the saturation properties of symmetric NM and give the nuclear incompressibility $K \approx 218$ and 252 MeV with the CDM3Y3 and CDM3Y6 versions, respectively. These interactions, especially the CDM3Y6 version, have been widely tested in the folding model analyses of the elastic nucleus-nucleus scattering [3–5]. The HF results for the ground-state energy of symmetric NM are shown in Fig. 1. One can see that at high NM densities the E/A curve obtained with the CDM3Y6 interaction is stiffer than that obtained with the CDM3Y3 interaction, and this is due to the higher value of the nuclear incompressibility K given by the CDM3Y6 interaction.

Given the parametrization (11) of the central (isoscalar) NN interaction, the HF part of the single-nucleon potential can be
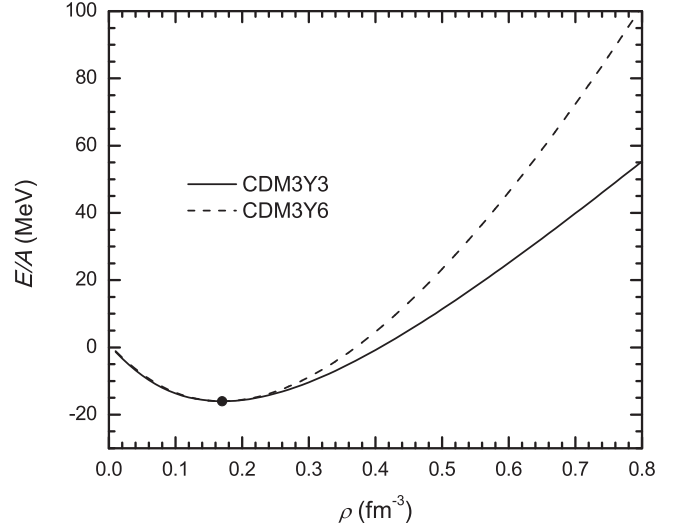

FIG. 1. Ground-state energy (per nucleon) of symmetric NM at different nucleon densities given by the HF calculation (1)–(2), using the CDM3Y3 and CDM3Y6 interactions (11). The solid circle is the saturation point ($E/A \approx -15.9$ MeV at $\rho_0 \approx 0.17$ fm^{-3}).

explicitly obtained as

$$U_{HF}(\rho,k) = F_0(\rho)U_{M3Y}(\rho,k),$$

where $\quad U_{M3Y}(\rho,k) = \rho\left[J_0^D + \int \hat{j}_1(k_F r)j_0(kr)v_{00}^{EX}(r)d^3r\right].$
$$(13)$$

Here

$$J_0^D = \int v_{00}^D(r)d^3r,$$
$$\hat{j}_1(x) = 3j_1(x)/x = 3(\sin x - x\cos x)/x^3.$$

Applying the HvH theorem, the RT of the single-nucleon potential in symmetric NM is obtained explicitly at the Fermi momentum as

$$U_{RT}(\rho,k_F) = \frac{\rho^2}{2}\frac{\partial F_0(\rho)}{\partial\rho}\left\{J_0^D + \int[j_1(k_F r)]^2 v_{00}^{EX}(r)d^3r\right\}.$$
$$(14)$$

It is obvious from Eq. (14) that the RT becomes zero if the original density independent M3Y interaction is used in the HF calculation of the single-nucleon potential. In this case, the HvH theorem is satisfied already on the HF level [16].

In general, as seen from Eq. (7), the RT of the nucleon mean-field potential should be present at arbitrary nucleon momenta. Microscopically, the momentum dependence of the RT was shown, in the Brueckner-Hartree-Fock (BHF) calculations of NM [23,24], to be due to the higher-order NN correlation, like the second-order diagram in the perturbative expansion of the mass operator or the contribution from three-body forces, etc. In finite nuclei, the rearrangement effect in the nucleon removal reactions was shown [21] to be strongly dependent on the energy of the stripping reaction, a clear indication of the momentum dependence of the RT of the single-nucleon potential. Therefore, it is of interest to assess the momentum

dependence of the RT of the single-nucleon potential on the HF level. Given the factorized density dependence of the CDM3Y3 and CDM3Y6 interactions, we have suggested recently [17] a compact method to account for the momentum dependence of the RT of the single-nucleon potential on the HF level. An important constraint for this procedure is that the momentum dependence of the total (HF+RT) single-nucleon potential reproduces the observed energy dependence of the nucleon OP. It was shown earlier [11,12] that the momentum dependence of the HF potential (13) accounts fairly well for the observed energy dependence of the nucleon OP after a slight adjustment of the interaction strength at high energies. Therefore, in our extended HF formalism [17] the *momentum dependent* RT of the single-nucleon potential is assumed to have a functional form similar to (13)

$$U_{\mathrm{RT}}(\rho,k) = \Delta F_0(\rho) U_{\mathrm{M3Y}}(\rho,k), \quad (15)$$

where the density dependent contribution of the rearrangement effect is determined consistently from the exact expression (14) of the RT at the Fermi momentum as

$$\Delta F_0(\rho) = \frac{U_{\mathrm{RT}}(\rho,k_F)}{U_{\mathrm{M3Y}}(\rho,k \to k_F)}. \quad (16)$$

Consequently, the total single-nucleon potential is determined in the extended HF approach as

$$U(\rho,k) = [F_0(\rho) + \Delta F_0(\rho)]U_{\mathrm{M3Y}}(\rho,k). \quad (17)$$

Thus, the momentum dependence of the total single-nucleon potential is determined by that of the exchange term of $U_{\mathrm{M3Y}}(\rho,k)$. One can see from the expressions (15)–(17) that the rearrangement effect gives rise to a modified density dependence of the central interaction (11), $F_0(\rho) \to F_0(\rho) + \Delta F_0(\rho)$, and the total (HF+RT) single-nucleon potential (17) is readily obtained on the HF level. The density dependence of $\Delta F_0(\rho)$ obtained from the exact expression of the RT given by the HvH theorem at each NM density using Eq. (16) is shown as squares and circles in Fig. 2. One can see that the behavior of $\Delta F_0(\rho)$ at high NM densities is quite different for the two density dependent CDM3Yn interactions and this is associated with different NM incompressibilities K given by these two interactions in the HF calculation of NM. Because $\Delta F_0(\rho) < 0$ over the whole range of NM densities, the contribution of the RT to the total single-nucleon potential is always repulsive. To facilitate the numerical calculation in the DFM, we have parametrized $\Delta F_0(\rho)$ using the a density dependent functional similar to (12):

$$\Delta F_0(\rho) = C[\alpha \exp(-\beta\rho) - 1]. \quad (18)$$

For convenience of the readers who are interested in using the modified CDM3Yn interaction (with the rearrangement contribution $\Delta F_0(\rho)$ added) in their folding model calculation, the parameters of $F_0(\rho)$ and $\Delta F_0(\rho)$ are given explicitly in Table I.

In the NM limit, the nucleon OP is determined as the mean-field interaction between the nucleon incident on NM at a given energy E and bound nucleons in the filled Fermi sea [12]. Applying a *continuous* choice for the single-nucleon potential [28] at positive energies E, we obtain in the HF scheme the
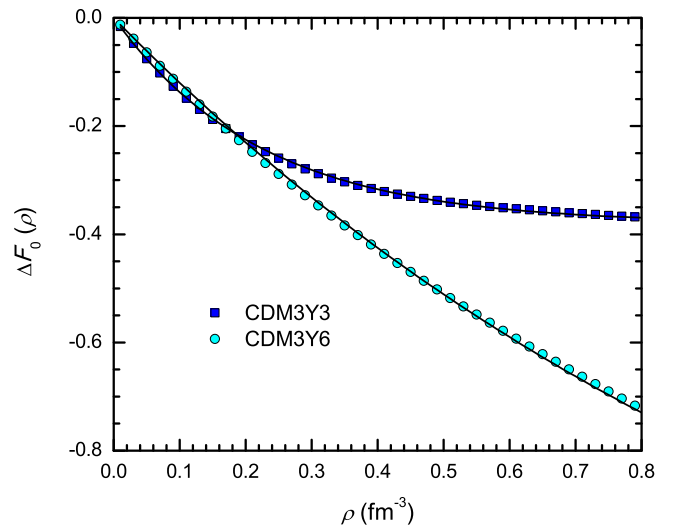

FIG. 2. Density dependence $\Delta F_0(\rho)$ of the RT (15) obtained from the exact expression of the RT given by the HvH theorem (14) using Eq. (16). Results obtained with the CDM3Y3 and CDM3Y6 interactions are shown as squares and circles, respectively. The solid curves are given by the density dependent functional (18) using the parameters in Table I.

nucleon OP in *symmetric* NM [11,12] as

$$U_0(\rho,E) = U_{\mathrm{HF}}(\rho,E)$$
$$= F_0(\rho)\rho\left[J_0^D + \int \hat{j}_1(k_F r)j_0(k(E,\rho)r)v_{00}^{\mathrm{EX}}(r)d^3r\right]. \quad (19)$$

Here $k(E,\rho)$ is the (energy dependent) momentum of the incident nucleon propagating in the mean field of bound nucleons, and is determined as

$$k(E,\rho) = \sqrt{\frac{2m}{\hbar^2}[E - U_0(\rho,E)]}, \quad \text{with } E > 0. \quad (20)$$

It is easy to see that $k(E,\rho) > k_F$ and U_{HF} is just the high momentum part of the HF potential (13). Based on the above discussion, the total nucleon OP in the NM should also have a contribution from the RT added:

$$U_0(\rho,E) = U_{\mathrm{HF}}(\rho,E) + U_{\mathrm{RT}}(\rho,E)$$
$$= [F_0(\rho) + \Delta F_0(\rho)]U_{\mathrm{M3Y}}(\rho,k(E,\rho)), \quad (21)$$

TABLE I. Parameters of the density dependence $F_0(\rho)$ of the CDM3Yn interaction (12) and the correction $\Delta F_0(\rho)$ by the RT of the single-nucleon potential (18). The nuclear incompressibility K is obtained in HF calculation of symmetric NM at the saturation density $\rho_0 \approx 0.17$ fm^{-3}.

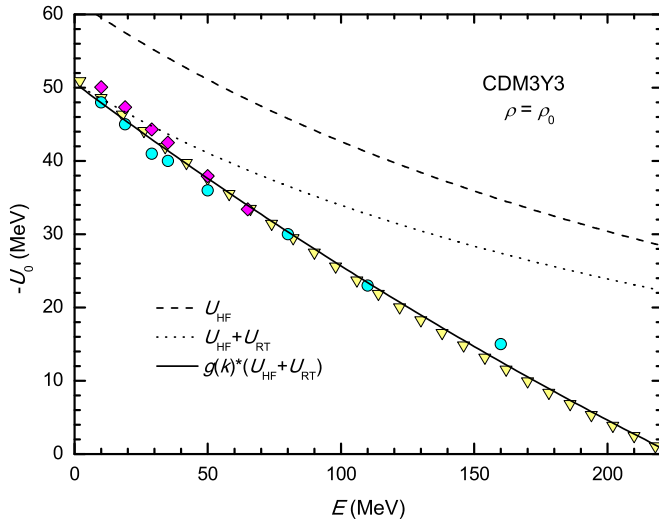| Interaction		C	α	β (fm^3)	γ (fm^3)	K (MeV)
CDM3Y3	$F_0(\rho)$	0.2985	3.4528	2.6388	−1.5	218
	$\Delta F_0(\rho)$	0.38	1.0	4.484		
CDM3Y6	$F_0(\rho)$	0.2658	3.8033	1.4099	−4.0	252
	$\Delta F_0(\rho)$	1.50	1.0	0.833		

FIG. 3. Nucleon OP in symmetric NM, evaluated using the CDM3Y3 interaction at the saturation density ρ_0 with and without the RT, in comparison with the empirical data taken from Refs. [25] (circles), [26] (squares), and [27] (triangles). The momentum dependent factor $g(k)$ was iteratively adjusted to the best agreement of the total nucleon OP (22) with the empirical data (solid line).
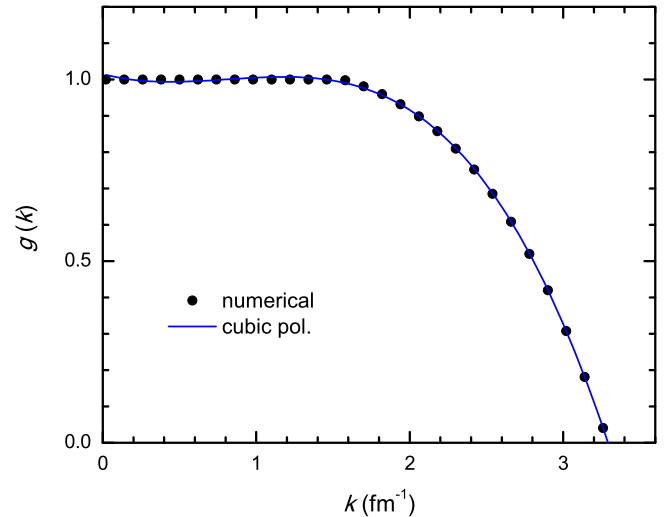

FIG. 4. Momentum dependent scaling factor $g(k)$ obtained with the CDM3Yn interaction from the best fit of the total nucleon OP (22) to the empirical data [27] shown in Fig. 3. The points are the numerical results that are well reproduced by a cubic polynomial, $g(k) = 1.015 - 0.109k + 0.17k^2 - 0.07k^3$ (the solid line).

where the density dependence $\Delta F_0(\rho)$ of the RT is determined by the relation (16) and parametrized in Table I.

The total nucleon OP (21) evaluated at the NM saturation density ρ_0 using the CDM3Y3 interaction is compared with the empirical data [25–27] in Fig. 3. Although the inclusion of the RT significantly improves the agreement of the calculated U_0 with the data at lowest energies, it remains somewhat more attractive at high energies in comparison with the empirical data. This effect is easily understood in light of the microscopic BHF results for the nucleon OP [28], where the energy dependence of the nucleon OP in NM was shown to originate from both the (energy dependent) direct and exchange parts of the Brueckner G matrix. That is the reason why a slight linear energy dependence has been introduced into the CDM3Y6 interaction [3], in terms of the $g(E)$ factor. To be consistent with the momentum dependence of the single-nucleon potential under study, instead of the $g(E)$ factor, we have introduced recently [17] a momentum (or energy) dependent scaling factor $g(k(E,\rho))$ to the CDM3Yn interaction (11), and iteratively adjusted its strength to the best agreement of the (HF+RT) nucleon OP with the empirical data at the NM saturation density ρ_0 (see Fig. 3). Thus,

$$U_0(\rho,E) = g(k(E,\rho))[F_0(\rho) + \Delta F_0(\rho)]U_{\text{M3Y}}(\rho,k(E,\rho)),$$
$$(22)$$

where $k(E,\rho)$ is determined self-consistently from $U_0(E,\rho)$ via Eq. (20). At variance with the $g(E)$ factor fixed by the incident energy [3], the $g(k(E,\rho))$ scaling factor is a function of the (energy dependent) momentum of the incident nucleon (see Fig. 4), directly linked to the momentum dependence of the nucleon mean-field potential. Numerically, the obtained $g(k(E,\rho))$ function is almost identical for both the CDM3Y3 and CDM3Y6 interactions and can be considered as the

explicit momentum (or energy) dependence of the CDM3Yn interaction that allows the incident nucleon to feel the nucleon mean field during its interaction with nucleons bound in NM. Such a momentum dependence is of a similar nature as the momentum dependence of the G matrix in the microscopic BHF study of NM, which is determined self-consistently through the momentum dependence of the single-particle energies embedded in the denominator of the Bethe-Goldstone equation [24]. The technical difference here is that the k dependence of $g(k)$ is determined empirically from the best fit of the calculated nucleon OP (22) to the observed energy dependence of the nucleon OP. Because $g(k)$ becomes smaller unity at $k \gtrsim 1.6$ fm^{-1} (see Fig. 4), it has been used in our recent HF calculation [17] to adjust the high-momentum tail of the single-nucleon potential in NM.

III. DOUBLE-FOLDING MODEL OF THE NUCLEUS-NUCLEUS OPTICAL POTENTIAL

Given quite a strong rearrangement effect to the nucleon OP discussed above, it is of high importance to incorporate these effects in the many-body calculation of the nucleon-nucleus and nucleus-nucleus optical potentials. Based on the realistic treatment of the rearrangement effect and momentum dependence of the nucleon OP in the extended HF calculation of NM, a consistent inclusion of the RT into the single-folding calculation of the nucleon-nucleus OP for finite nuclei has been done [17] in the same mean-field manner, and the contribution of the RT was shown to be essential in obtaining the realistic shape and strength of the real nucleon OP. Because the double-folding model evaluates the nucleus-nucleus OP on the same HF-type level as the single-folding calculation of the nucleon-nucleus OP, the contribution of the RT to the total nucleus-nucleus potential is expected to be also significant. In the present work, we develop an extended version of the DFM to

effectively include the RT in the double-folding calculation of the nucleus-nucleus OP in a similar manner, using consistently the same density and energy dependent CDM3Yn interaction that was fine tuned to be compliant with the HvH theorem in the HF study of NM discussed in Sec. II.

We recall that in the DFM, the central nucleus-nucleus OP is evaluated as an HF-type potential [3,5] using an effective (energy and density dependent) NN interaction $v_c(\rho, E)$:

$$U_F(E,R) = \sum_{i \in a, j \in A} [\langle ij|v_c^D(\rho,E)|ij\rangle + \langle ij|v_c^{EX}(\rho,E)|ji\rangle],$$
(23)

where $|i\rangle$ and $|j\rangle$ are the single-particle wave functions of the projectile (a) and target (A) nucleons, respectively. The direct part of the double-folded potential (23) is local, and is expressed in terms of the ground-state (g.s.) densities of the two colliding nuclei as

$$U_F^D(E,R) = \int \rho_a(\boldsymbol{r}_a)\rho_A(\boldsymbol{r}_A)v_c^D(\rho,E,s)d^3r_a d^3r_A,$$
$$s = \boldsymbol{r}_A - \boldsymbol{r}_a + \boldsymbol{R}.$$
(24)

The antisymmetrization of the $a + A$ system is done by taking into account explicitly the knock-on exchange effects. As a result, the exchange term of U_F becomes nonlocal in the coordinate space [5]. An accurate local approximation is usually made by treating the relative motion locally as a plane wave [5], and the exchange part of the double-folded potential (23) can be obtained in the following *localized* form

$$U_F^{EX}(E,R) = \int \rho_a(\boldsymbol{r}_a, \boldsymbol{r}_a + s)\rho_A(\boldsymbol{r}_A, \boldsymbol{r}_A - s)$$
$$\times v_c^{EX}(\rho,E,s)\exp\left(\frac{i\boldsymbol{K}(E,R).s}{M}\right)d^3r_a d^3r_A,$$
(25)

where $\rho_{a(A)}(\boldsymbol{r}, \boldsymbol{r}')$ are the nonlocal g.s. density matrices, $M = aA/(a+A)$ is the recoil factor (or reduced mass number), with a and A being the mass numbers of the projectile and target, respectively. The local momentum $K(E,R)$ of the relative motion is determined self-consistently from the real nucleus-nucleus OP as

$$K^2(E,R) = \frac{2\mu}{\hbar^2}[E - U_F(E,R) - V_C(R)],$$
(26)

where μ is the reduced mass of the two nuclei and $V_C(R)$ is the Coulomb potential.

At low energies, the pair-wise interaction between the projectile nucleons and those in target can induce certain rearrangement of the single-particle configurations in both nuclei. Such impact by the rearrangement effect has been observed experimentally in the nucleon removal reactions [21]. In terms of the nucleus-nucleus interaction, the rearrangement effect should affect also the shape and strength of the nucleus-nucleus OP (23), constructed in the DFM using the single-particle wave functions of the projectile and target nucleons. Given the rearrangement contribution to the density dependence of the CDM3Yn interaction determined above in the HF study of the nucleon OP in NM, we have included the RT into the

double-folding calculation of the nucleus-nucleus OP (23) in the same manner as done earlier for the single-folding calculation of the nucleon OP [17]. Namely, the RT given by the correction $\Delta F_0(\rho)$ of the density dependence of the CDM3Yn interaction is added to the double-folded potential (23), so that the total folded nucleus-nucleus OP is obtained in the present DFM calculation as

$$U_F(E,R)$$
$$= U_F^D(E,R) + U_F^{EX}(E,R) + U_{RT}(E,R)$$
$$= g(k(E,R)) \int [F_0(\rho) + \Delta F_0(\rho)]\{\rho_a(\boldsymbol{r}_a)\rho_A(\boldsymbol{r}_A)v_{00}^D(s)$$
$$+ \rho_a(\boldsymbol{r}_a, \boldsymbol{r}_a + s)\rho_A(\boldsymbol{r}_A, \boldsymbol{r}_A - s)v_{00}^{EX}(s)$$
$$\times \exp(i\boldsymbol{k}(E,R)\cdot s)\}d^3r_a d^3r_A,$$
(27)

where the *average* local nucleon momentum in the nuclear mean field of the two interacting nuclei is given by $k(E,R) = K(E,R)/M$. One can see in Eq. (27) that the contribution of the RT is present in both the direct and exchange terms of the nucleus-nucleus OP. Because the correction $\Delta F_0(\rho)$ by the RT is parametrized in the density dependent form (18) similar to that of the CDM3Yn interaction (12), the double-folding integral (27) can be readily evaluated using the DFM developed earlier in Refs. [3–5,29], where the sum of the two g.s. densities of the colliding nuclei is adopted for the overlap density ρ appearing in $F_0(\rho) + \Delta F_0(\rho)$. Such a frozen density approximation (FDA) for the overlap density of the nucleus-nucleus system was discussed repeatedly in the past [1,3,5,29,30], and FDA was proven to be a reliable approximation at the (refractive) energies considered in the present study (see, e.g., results of the quantum molecular dynamics simulation of the $^{16}O + ^{16}O$ collision at 22 MeV/nucleon [29] where the overlap density in the compression stage is very close to that given by the FDA, or the comparison of the FDA and adiabatic density approximation in Ref. [30]). At low energies, especially, those of nuclear astrophysics interest, FDA is no longer accurate, and an appropriate adiabatic approximation for the overlap density should be used instead.

It can be seen from Eqs. (26) and (27) that the energy dependence of the nucleus-nucleus OP folded with the CDM3Yn interaction is entirely determined by the local nucleon momentum $k(E,R)$ that appears explicitly in the exchange term as well as in the local $g(k(E,R))$ factor. Given the $g(k)$ function determined above in the HF calculation of NM based on the observed energy dependence of the nucleon OP, the local $g(k(E,R))$ factor of the folded nucleus-nucleus potential (27) is interpolated from the $g(k)$ values in the NM limit (see Fig. 4) for each local nucleon momentum $k = k(E,R)$ determined self-consistently from Eq. (26) using an iterative procedure. Thus, $g(k(E,R))$ can be considered as the explicit energy dependence of the density dependent CDM3Yn interaction (11), *locally* consistent with the nuclear mean field based on the real folded nucleus-nucleus potential (27). This is an important new feature of the extended DFM compared to the earlier versions of the DFM [3,4] where a linear energy dependence $g(E)$ fixed by the incident energy was used to scale the CDM3Yn interaction.

IV. FOLDING MODEL ANALYSIS OF THE ELASTIC ^{12}C + ^{12}C AND ^{16}O + ^{12}C SCATTERING AT THE REFRACTIVE ENERGIES

In general, the elastic HI scattering is associated with the strong absorption [1] that suppresses the refractive (rainbow-like) structure of the elastic cross section. Therefore, most of the elastic HI scattering occurs at the surface and the measured elastic data carry little information about the nucleus-nucleus interaction potential at small distances ($R < R_{s.a.}$). However, the situation becomes different in cases of the refractive α-nucleus or light HI scattering, where the absorption is weak and the refractive structure of the nuclear rainbow appears at medium and large scattering angles, which enables the determination of the real nucleus-nucleus OP with a much less ambiguity, down to subsurface distances [5]. The nuclear rainbow pattern has been shown to be of the far-side scattering, and is usually preceded in angles by the Airy minima [5,7]. The observation of these minima, especially the first Airy minimum A1 that is immediately followed by a broad (shoulder-like) nuclear rainbow pattern, greatly facilitates the determination of the real OP [5,31,32]. It should be noted that the large-angle nuclear rainbow pattern observed in the (weak-absorbing) elastic α-nucleus or light HI scattering can be shown, using the semiclassical formalism of the elastic nucleus-nucleus scattering developed by Brink and Takigawa 40 years ago [33], to be associated with the *internal* wave that penetrates through the Coulomb + centrifugal barrier into the interior of the real nucleus-nucleus OP, while the forward (diffractive) part of the elastic cross section is associated with the *barrier* wave reflected from the barrier. As a result, the refractive (large-angle) elastic data are certainly sensitive to the real OP at small radii. In a further optical model (OM) study of the elastic ^{12}C + ^{12}C scattering at low energies, the broad (Airy-like) oscillation of the elastic cross section at medium and large angles was shown by Rowley *et al.* [34] to be due to the interference of the far-side components of both the barrier and internal waves. Such an interference scenario is very similar (in the physics interpretation) to the Airy interference pattern of the nuclear rainbow discussed later in Refs. [5,7,31,32].

We recall here that there is a window in the energy or a range of the refractive energies, where the prominent nuclear rainbow pattern associated with the first Airy minimum can be observed. If the energy is too low, the broad rainbow pattern following A1 occurs at very backward angles and might well be hindered by other interferences (like the Mott interference in the symmetric ^{12}C + ^{12}C and ^{16}O + ^{16}O systems or the elastic α transfer in the ^{16}O + ^{12}C system). On the other hand, if the energy is too high, both A1 and the rainbow maximum move forward to small scattering angles and the rainbow structure is destroyed by the interference of the near-side and far-side scatterings, leading to the Fraunhofer oscillation. For the incident ^{12}C and ^{16}O ions, this energy window is about 10 to 40 MeV/nucleon, i.e., around the Fermi energy. It should be noted that the Airy interference pattern was also confirmed in the OM analyses [34,35] of the elastic ^{12}C + ^{12}C scattering data at lower energies ($E < 10$ MeV/nucleon) [36,37]. In the present work, we concentrate mainly on the evolution of the broad nuclear rainbow pattern associated with A1, and

the extended DFM is used to calculate the real OP for the OM analysis of the elastic ^{12}C + ^{12}C and ^{16}O + ^{12}C scattering data at the refractive energies.

Like the earlier folding model studies of these data [3,29,38–40], the (energy dependent) folded potential (27) enters the OM calculation as the real OP and the imaginary part of the OP is assumed to be in the standard Woods-Saxon (WS) form. Thus, the total OP at the internuclear distance R is determined as

$$U(R) = N_R U_F(E, R) - \frac{i W_V}{1 + \exp[(R - R_V)/a_V]} + V_C(R).$$
(28)

The Coulomb part of the optical potential $V_C(R)$ is obtained by directly folding two uniform charge distributions [41], chosen to have RMS charge radii $R_C = 3.17$ and 3.54 fm for ^{12}C and ^{16}O ions, respectively. Such a choice of the Coulomb potential was shown to be accurate up to small internuclear radii where the nuclear interaction becomes dominant [7]. The g.s. nuclear densities of ^{16}O and ^{12}C used in the present DFM calculation were taken as Fermi distributions with parameters [30] chosen to reproduce the empirical matter radii of these nuclei. All the OM analyses were made using the code ECIS97 written by Raynal [42], with relativistically corrected kinematics. The renormalization factor N_R of the real folded potential and WS parameters were adjusted in each case to the best agreement of the calculated elastic cross section with the measured elastic data, while keeping the shape of the complex OP within a consistent mean-field description.

A. ^{12}C + ^{12}C system

Among numerous experiments on elastic HI scattering, ^{12}C + ^{12}C is perhaps the most studied system, with the elastic scattering measured at energies ranging from the Coulomb barrier up to 200 MeV/nucleon. This is a strongly refractive system, with the energy dependent Airy structure of the nuclear rainbow well established. The elastic ^{12}C + ^{12}C scattering data measured at different energies, over a wide angular range, enabled the determination of the real OP with much less ambiguity. The deep family of the real OP for this system (which is quite close to that predicted by the folding model [7]) gives a realistic evolution of the Airy minima shaping the famous "Airy elephants" in the 90° excitation function at low energies, where the prominent minimum at 102 MeV in the 90° excitation function is due to the second Airy minimum A2 passing through $\theta_{c.m.} \approx 90°$ at that energy [35]. The elastic ^{12}C + ^{12}C scattering was shown to be dominated by the far-side scattering at energies ranging from a few MeV/nucleon [34,38] up to 200 MeV/nucleon [43]. In the present work we consider selectively six data sets of the elastic ^{12}C + ^{12}C scattering measured at the incident energies of 139.5, 158.8, 240, 288.6, 360, and 1016 MeV [44–48], which were shown in the earlier OM and folding model analyses [3,7,29,38,39] as sensitive to the strength and shape of the real OP at both the surface and subsurface distances. In particular, the experiments on the ^{12}C + ^{12}C scattering at $E_{lab} = 139.5$, 158.8 [44], and

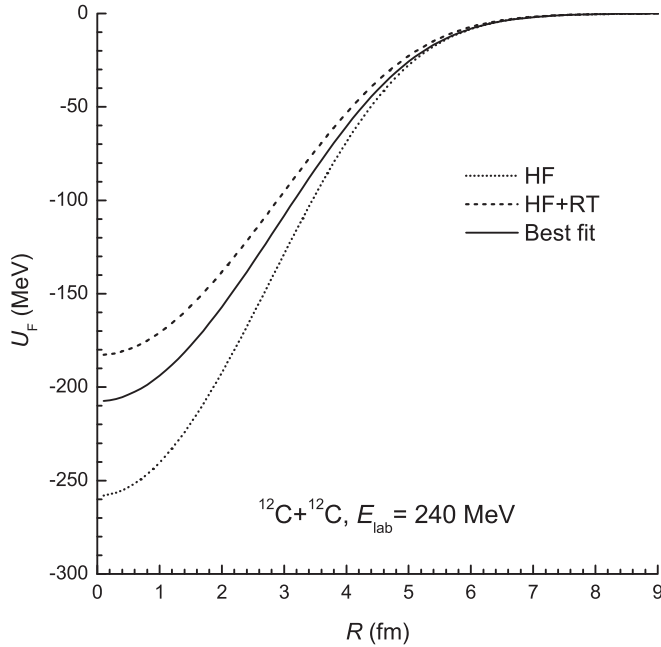FIG. 5. Unrenormalized total (HF+RT) folded potential (27) obtained with the CDM3Y3 interaction for the elastic ^{12}C+^{12}C scattering at $E_{lab} = 240$ MeV (dashed line) in comparison with that obtained on the HF level only (dotted line), and the folded potential renormalized by the N_R factor (solid line) determined from the best OM fit to the data (see Table II).

240 MeV [45,46] were aimed at revealing as clearly as possible the nuclear rainbow pattern.

In the present work we focus on the impact of the rearrangement effect and momentum dependence of the nucleon mean-field potential in the folding model description of the refractive ^{12}C+^{12}C scattering. As shown earlier for the folded nucleon OP, the rearrangement effect of the nucleon mean field gives rise to a strong repulsive contribution of the RT to the real folded potential at small radii [17]. It is clear from Fig. 2 that the higher the nuclear density the stronger the effect

caused by the RT. In case of the double-folded nucleus-nucleus potential, the overlap nuclear density is well above ρ_0 at small internuclear distances and the repulsive contribution by the RT is quite strong there. The (unrenormalized) total (HF+RT) real folded potential (27) obtained with the CDM3Y3 interaction for the ^{12}C+^{12}C system at $E_{lab} = 240$ MeV is compared with the HF folded potential in Fig. 5, and one can see that the repulsive contribution of the RT is up to about 30–40% of the potential strength at the smallest radii. In the same direction, the best OM fit to the elastic ^{12}C+^{12}C data at different energies requires also a shallower real OP compared to the deep HF folded potential, which needs to be renormalized by a factor $N_R \approx 0.7$–0.8 for the best OM description of the data (see Table II). For the ^{12}C+^{12}C system at the considered energies, the impact of the RT is slightly too repulsive and the total (HF+RT) folded potential needs to be renormalized by a factor $N_R \approx 1.1$–1.2 for the best OM description of the data. We emphasize that the best-fit parameters of the OP presented in Table II allow one to properly describe the Airy structure of the nuclear rainbow pattern observed for the ^{12}C+^{12}C system, using the CDM3Y3 folded potential. Using the real folded potential based on the CDM3Y6 interaction, we obtained N_R values about 5% larger than those obtained with the CDM3Y3 interaction and nearly the same WS parameters for the imaginary WS potential. Such a subtle effect is associated with a higher nuclear incompressibility K given by the CDM3Y6 interaction in the HF calculation of NM, which results in a slightly more repulsive contribution of the RT to the total folded potential.

The elastic ^{12}C+^{12}C scattering at 240 MeV is quite an interesting case (see Fig. 6). The first measurement of the elastic cross section at this energy [45] was done for angles up to $\theta_{c.m.} \approx 55°$ only, and the folding model analysis [29,38] suggested that the first Airy minimum (A1) is located at $\theta_{c.m.} \approx 41°$ and followed by a broad (shoulder-like) rainbow pattern. However, an alternative scenario for the Airy structure in the ^{16}O+^{12}C and ^{12}C+^{12}C systems has been proposed [49] where the minimum observed in the elastic ^{12}C+^{12}C cross section at around 41° is the second Airy minimum (A2),

TABLE II. The best-fit parameters of the OP (28) for the elastic ^{12}C+^{12}C scattering at $E_{lab} = 139.5$–1016 MeV. N_R is the best-fit renormalization factor of the real CDM3Y3 folded potential, J_R and J_W are the volume integrals (per interacting nucleon pair) of the real and imaginary parts of the OP, respectively. σ_R is the total reaction cross section.

| E_{lab} (MeV)	Real OP	N_R	J_R (MeV fm^3)	W_V (MeV)	R_V (fm)	a_V (fm)	J_W (MeV fm^3)	σ_R (mb)
139.5	HF	0.810	325.5	26.60	5.170	0.600	121.2	1393
	HF+RT	1.100	343.8	27.00	5.270	0.600	129.7	1443
158.8	HF	0.805	320.3	22.51	5.248	0.707	116.6	1514
	HF+RT	1.101	337.7	23.25	5.290	0.740	119.5	1596
240	HF	0.815	311.9	24.02	5.425	0.645	127.1	1485
	HF+RT	1.135	334.1	23.74	5.548	0.678	135.8	1596
288.6	HF	0.805	300.7	26.73	5.122	0.715	124.6	1469
	HF+RT	1.100	315.7	26.71	5.249	0.717	133.1	1519
360	HF	0.693	250.3	22.91	5.180	0.672	108.0	1356
	HF+RT	0.980	271.0	23.54	5.240	0.718	117.4	1455
1016	HF	0.670	183.8	17.09	5.171	0.802	85.03	1192
	HF+RT	1.090	205.5	17.19	5.344	0.709	89.57	1187
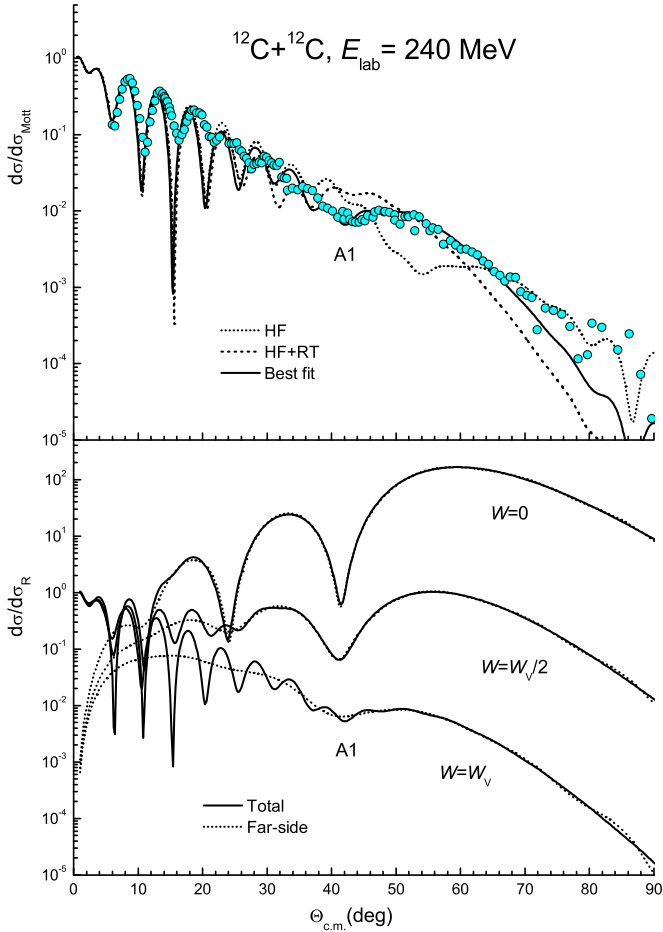
FIG. 6. Upper part: OM description of the elastic $^{12}C + ^{12}C$ scattering data at $E_{lab} = 240$ MeV [45,46] given by three choices of the real folded potential (27) shown in Fig. 5, using the best-fit imaginary OP taken from Table II. Lower part: Total unsymmetrized elastic $^{12}C + ^{12}C$ scattering cross section at 240 MeV (solid lines) and contribution of the far-side scattering (dotted lines) given by the best-fit real folded potential with different absorptive strengths of the WS imaginary potential taken from Table II. A1 denotes the first Airy minimum that is followed by the broad (shoulder-like) rainbow pattern.

and the first Airy minimum A1 should occur at larger angles ($\theta_{c.m.} \approx 60°$). To clarify the situation, a further experiment on the elastic $^{12}C + ^{12}C$ scattering at 240 MeV has been done using the kinematical coincidence method [46]. The elastic $^{12}C + ^{12}C$ scattering cross section measured up $\theta_{c.m.} \approx 90°$ (see upper part of Fig. 6) shows clearly no refractive minimum in the angular region $\theta_{c.m.} \approx 60° - 70°$. Therefore, A1 is now firmly established at $\theta_{c.m.} \approx 41°$ for the elastic $^{12}C + ^{12}C$ scattering at 240 MeV. As shown repeatedly in the earlier OM studies of elastic $^{12}C + ^{12}C$ scattering [29,35,38], locations of the Airy minima are mainly determined by the strength of the real OP at small radii. One can see in Fig. 5 that the (deeper) HF folded potential gives A1 located at $\theta_{c.m.} \approx 54°$ for the $^{12}C + ^{12}C$ system at 240 MeV, while A1 given by the (shallower) HF+RT folded potential is shifted forward to around $38°$. The best OM fit to these data given by the renormalized real

folded potential and the WS imaginary potential (see Table II) reproduces the first Airy minimum around that observed in experiment at $\theta_{c.m.} \approx 41°$. Note that the best-fit elastic cross sections given by both the renormalized HF and HF+RT folded potentials are graphically the same as shown in upper part of Fig. 6. Although the Airy structure of the nuclear rainbow is shaped by the real OP, its oscillating pattern is frequently obscured by the absorptive imaginary OP (or by the absorption of the incident flux into different nonelastic channels). To illustrate the refractive (far-side scattering) structure of the elastic $^{12}C + ^{12}C$ scattering at this interesting energy, we have performed the unsymmetrized OM calculation of the elastic cross section (neglecting the Mott symmetrization required for the identical $^{12}C + ^{12}C$ system, to avoid the Mott oscillation of the elastic cross section at angles around $90°$) using the best-fit HF+RT folded potential with different absorptive strengths of the WS imaginary OP taken from Table II. The elastic cross section was further decomposed in terms of the near-side and far-side scattering cross sections using Fuller's method [50], and one can see in the lower part of Fig. 6 that the location of the first Airy minimum and the broad rainbow pattern that follows A1 are determined entirely by the far-side scattering amplitude, which in turn is determined mainly by the radial shape of the real OP. That is the reason why the accurate data of the nuclear rainbow scattering are indispensable in probing the strength and shape of the real nucleus-nucleus OP [5,7].

At the lower incident energies of 139.5 and 158.8 MeV, because of the Mott interference at the scattering angles from $\theta_{c.m.} \approx 70°$ to beyond $90°$, one cannot clearly allocate the Airy minima from the extensive data measured by Kubono *et al.* [44]. Only the unsymmetrized OM calculation with different absorptive strengths could help to resolve that (see Fig. 7), and the first Airy minimum A1 was found at $\theta_{c.m.} \approx 78°$ and $66°$ at the energies of 139.5 and 158.8 MeV, respectively. With the incident energies increasing to 288.6 and 360 MeV, A1 is shifted to the forward angles (see Fig. 8). A near-far decomposition of the scattering amplitude with a weaker absorption reveals the A1 location at $\theta_{c.m.} \approx 31°$ and $20°$ at $E_{lab} = 288.6$ and 360 MeV, respectively. One can see that the rainbow pattern associated with the first Airy minimum begins to be obscured by the near-far interference at 360 MeV. At the higher energy of $E_{lab} = 1016$ MeV, the far-side scattering is still dominant at large angles, but becomes much weaker at the most forward angles where the scattering cross section shows a typical oscillation resulting from the interference of the near-side and far-side scattering amplitudes. Given a realistic (mean-field based) energy dependence of the CDM3Yn interaction via $g(k(E, R))$ factor [see Eqs. (26) and (27)], the best-fit N_R values obtained for the real HF+RT folded potential turned out to be around unity at the high energies of $E_{lab} = 360$ and 1016 MeV, while those obtained for the real HF folded potential are below 0.7 (see Table II).

Thus, we have shown that the evolution of the Airy structure in the elastic $^{12}C + ^{12}C$ scattering at the energies of 12 to 85 MeV/nucleon is well described by the real folded potential based on the modified density and energy dependent CDM3Yn interaction that properly takes into account the rearrangement effect. With a strong impact of the RT to the nucleon mean-field potential at low energies [17], the extended DFM should be
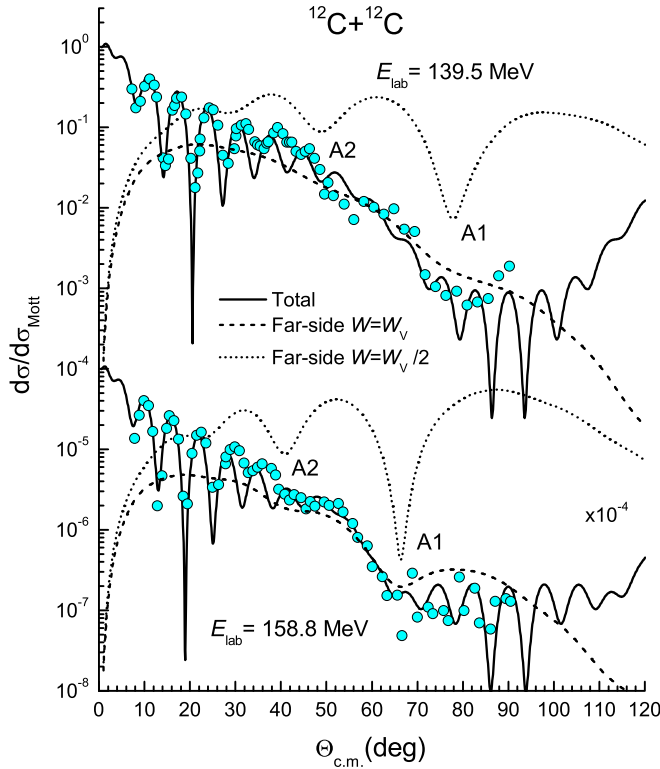
FIG. 7. OM description of the elastic $^{12}C + ^{12}C$ scattering data at $E_{lab} = 139.5$ and 158.8 MeV [44] given by the best-fit (HF+RT) real folded potential and WS imaginary potential taken from Table II (solid lines). The far-side scattering cross sections are given by the unsymmetrized OM calculation using the same real folded OP but with different absorptive strengths W_V of the WS imaginary potential (dashed and dotted lines). Ak is the kth order Airy minimum

FIG. 8. The same as Fig. 7 but for the elastic $^{12}C + ^{12}C$ scattering data measured at $E_{lab} = 288.6$, 360, and 1016 MeV [47,48].

further used in the OM study of the elastic $^{12}C + ^{12}C$ scattering at low energies, to pin down the potential ambiguity in the low-energy regime and improve the consistent mean-field description of the elastic scattering and shape resonances in the $^{12}C + ^{12}C$ system [51].

B. $^{16}O + ^{12}C$ system

Although the $^{12}C + ^{12}C$ system was shown above as strongly refractive, the Mott interference caused by the boson symmetry between the two identical ^{12}C nuclei leads to rapidly oscillating elastic cross section at angles around $\theta_{c.m.} = 90°$, which obscures the Airy structure in this angular region. As shown above in Figs. 6–8, the whole Airy pattern can be clearly seen only in the unsymmetrized OM calculation that removes the Mott interference artificially. The $^{16}O + ^{12}C$ system does not have the boson symmetry, and was suggested 25 years ago by Brandan and Satchler [52] as a good candidate for the study of the nuclear rainbow. Since the late 1990s, continuing efforts have been made by the Kurchatov-institute group to accurately measure the elastic $^{16}O + ^{12}C$ scattering at the refractive energies ($E_{lab} = 132$ to 330 MeV) using the heavy-ion accelerators of both the Kurchatov institute and Jyväskylä University [40,49,53,54]. In the present work we consider the elastic $^{16}O + ^{12}C$ scattering data measured at
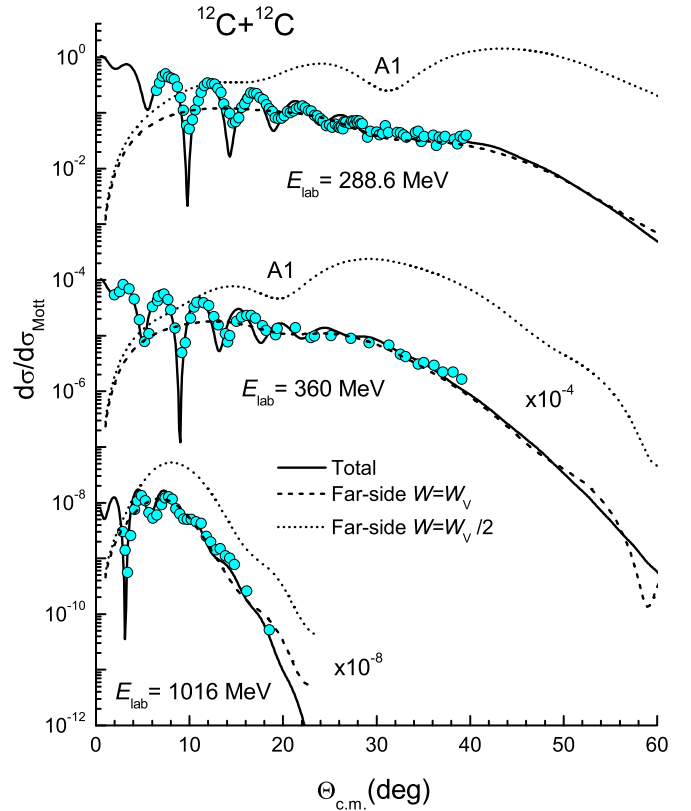
the incident energies of 132, 170, 200, 230, 260, 281, and 330 MeV by the Kurchatov group [40,54] which exhibit a quite prominent Airy structure of the nuclear rainbow, and the elastic $^{16}O + ^{12}C$ scattering data measured at $E_{lab} = 300$ and 608 MeV by Brandan *et al.* [55,56]. To study the energy dependence of the OP of the $^{16}O + ^{12}C$ system, the elastic data measured at $E_{lab} = 1503$ MeV [57] were also analyzed in the present work.

Among different elastic data measured at the refractive energies, the elastic $^{16}O + ^{12}C$ scattering data at $E_{lab} = 200$ MeV [40] are perhaps the most prominent example of the nuclear rainbow observed in the light HI scattering. The (unrenormalized) HF and HF+RT real folded potential (27) obtained with the CDM3Y3 interaction for the $^{16}O + ^{12}C$ system at 200 MeV are shown in Fig. 9. As observed above for the $^{12}C + ^{12}C$ system, the repulsive contribution of the RT to the real folded $^{16}O + ^{12}C$ potential is up to about 40% of the potential strength at the smallest radii. The best OM fit to the elastic $^{16}O + ^{12}C$ data at this energy also implies a real OP significantly shallower than the HF folded potential. It is remarkable that in the $^{16}O + ^{12}C$ case, the best-fit renormalization coefficient N_R for the HF+RT folded potential is very close to unity, while that obtained for the HF potential is $N_R \approx 0.72$–0.75 (see Table III). This shows that the real folded potential obtained in the extended DFM with the RT properly taken into account has a much improved predicting power for the real nucleus-nucleus OP, and the Airy structure of the elastic angular distribution observed
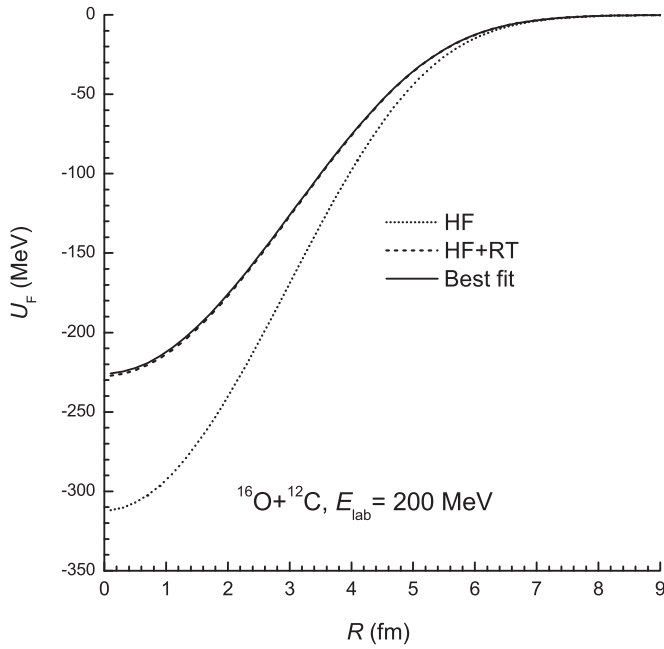
FIG. 9. Unrenormalized total real HF+RT folded potential (27) obtained with the CDM3Y3 interaction for the elastic ^{16}O$+^{12}$C scattering at $E_{lab} = 200$ MeV (dashed line) in comparison with that obtained on the HF level only (dotted line), and the real HF+RT folded potential renormalized by the best-fit N_R factor taken from Table III (solid line).

for the ^{16}O$+^{12}$C system at the considered energies can be reproduced rather well, using the unrenormalized real HF+RT folded potential. The results of our folding model analysis of the elastic ^{16}O$+^{12}$C scattering at $E_{lab} = 200$ MeV shown in Fig. 10 illustrate very well the reliability of the HF+RT folded potential. Without the contribution of the RT, the HF folded potential is rather deep and wrongly predicts the first Airy minimum at $\theta_{c.m.} \approx 101°$ for the ^{16}O$+^{12}$C system at 200 MeV. The shallower HF+RT folded potential shifts A1 forward to $\theta_{c.m.} \approx 69°$ as observed in the experiment. The best OM fit to these data resulted in the renormalization factors $N_R \approx 0.72$ and 0.99 for the HF and HF+RT folded potentials, respectively. Not distorted by the Mott interference as in the ^{12}C$+^{12}$C case, the measured elastic ^{16}O$+^{12}$C cross section at 200 MeV exhibits a broad shoulder-like rainbow pattern that spreads well over the angles beyond 100°. As a result, the elastic ^{16}O$+^{12}$C data measured at this energy can serve as a very good probe of the real OP for the ^{16}O$+^{12}$C system. Given much less ambiguity of the real OP in this case, the strength and shape of the HF+RT folded potential (with the best-fit N_R factor close to unity) turn out to be quite close to those implied by the realistic OM description of the Airy structure observed in the elastic ^{16}O$+^{12}$C scattering data at 200 MeV [40]. The strength of the HF folded potential needs to be scaled down by about 30% to give a proper description of the first Airy minimum and the shoulder-like rainbow pattern that follows A1. Such a difference in the strength of the folded potential seems to be well accounted for by the repulsive contribution of the rearrangement term.

TABLE III. The best-fit parameters of the OP (28) for the elastic ^{16}O$+^{12}$C scattering at $E_{lab} = 132$–1503 MeV. N_R is the best-fit renormalization factor of the real CDM3Y3 folded potential, J_R and J_W are the volume integrals (per interacting nucleon pair) of the real and imaginary parts of the OP, respectively. σ_R is the total reaction cross section.

| E_{lab} (MeV)	Real OP	N_R	J_R (MeV fm^3)	W_V (MeV)	R_V (fm)	a_V (fm)	J_W (MeV fm^3)	σ_R (mb)
132	HF	0.757	316.5	13.31	5.937	0.642	67.81	1547
	HF+RT	1.017	331.7	14.67	5.772	0.751	71.80	1661
170	HF	0.741	305.3	17.69	5.913	0.579	87.80	1559
	HF+RT	1.006	323.4	17.30	6.057	0.600	91.96	1624
181	HF	0.731	299.9	20.99	5.618	0.650	91.94	1561
	HF+RT	0.987	315.9	20.91	5.733	0.650	96.87	1614
200	HF	0.723	294.5	18.26	5.959	0.550	91.41	1527
	HF+RT	0.994	315.9	17.33	6.160	0.530	94.82	1579
230	HF	0.726	292.4	21.02	5.776	0.597	97.71	1547
	HF+RT	0.985	309.5	20.44	5.923	0.589	101.7	1597
260	HF	0.716	285.2	21.99	5.740	0.555	99.11	1485
	HF+RT	0.965	299.7	21.46	5.867	0.576	103.5	1563
281	HF	0.707	279.4	22.58	5.685	0.552	98.93	1462
	HF+RT	0.959	295.5	22.01	5.821	0.572	103.7	1542
300	HF	0.715	280.6	26.82	5.535	0.634	112.1	1550
	HF+RT	0.960	293.6	26.37	5.630	0.680	117.4	1655
330	HF	0.700	271.7	26.28	5.490	0.602	106.2	1476
	HF+RT	0.945	285.7	24.99	5.653	0.600	109.4	1532
608	HF	0.663	233.4	22.53	5.532	0.579	92.23	1359
	HF+RT	0.915	247.7	21.48	5.745	0.586	97.96	1444
1503	HF	0.671	179.5	19.01	5.511	0.758	82.38	1318
	HF+RT	1.022	213.0	15.90	5.823	0.627	76.32	1262
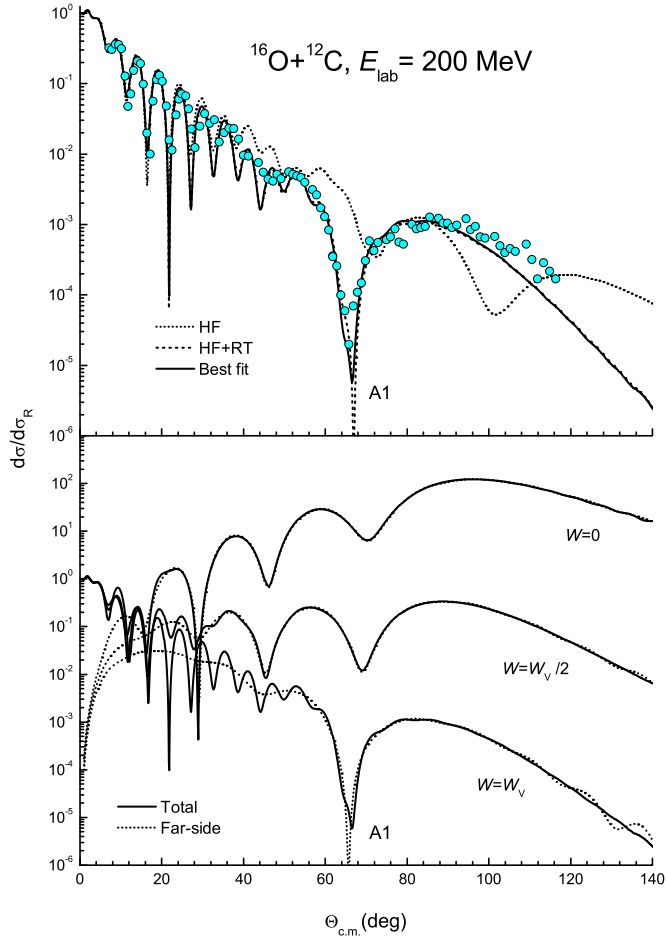
FIG. 10. Upper part: OM description of the elastic $^{16}O + ^{12}C$ scattering data at $E_{lab} = 200$ MeV [40] given by three choices of the real folded potential (27) shown in Fig. 9, using the best-fit imaginary OP taken from Table III. Lower part: Total elastic $^{16}O + ^{12}C$ scattering cross section at 200 MeV (solid lines) and contribution of the far-side scattering (dotted lines) given by the best-fit real HF+RT folded potential with different absorptive strengths of the WS imaginary potential taken from Table III. A1 denotes the first Airy minimum that is followed by the broad (shoulder-like) rainbow pattern.

The OM description of the elastic $^{16}O + ^{12}C$ scattering data at the lower energies of $E_{lab} = 132$, 170, and 181 MeV is shown in Fig. 11. The best fit to these data has been achieved with the CDM3Y3 folded HF and HF+RT potentials renormalized by factors $N_R \approx 0.73$–0.76 and $N_R \approx 0.99$–1.02, respectively. This confirms again the important (repulsive) contribution of the RT to the $^{16}O + ^{12}C$ folded potential that helps to improve the prediction of the real OP by the extended DFM. The best-fit real folded potential also reproduces nicely the Airy oscillation established earlier in the detailed OM analysis of these data [40]. At 132 MeV, the most prominent are the second (A2) and third (A3) Airy minima observed at $\theta_{c.m.} \approx 83°$ and $56°$, respectively. At this low energy, the first Airy minimum A1 is located beyond $\theta_{c.m.} = 120°$, and is totally obscured by the oscillating cross section at large angles that is likely due to the elastic α and nucleon transfer processes [58–60]. The folded HF+RT potential could be used as the bare $^{16}O + ^{12}C$ potential
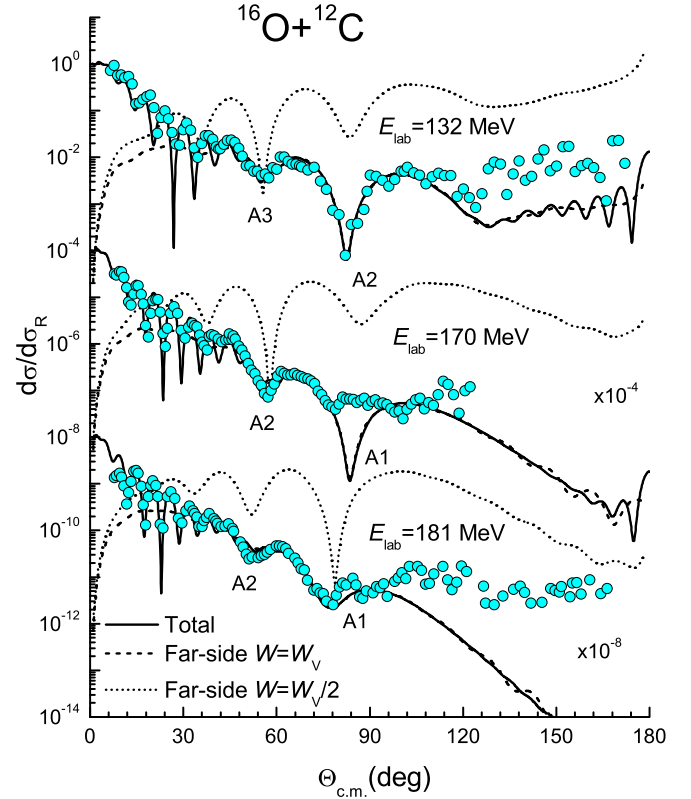

FIG. 11. OM description of the elastic $^{16}O + ^{12}C$ scattering data at $E_{lab} = 132$, 170, and 181 MeV [40,49,54] given by the best-fit (HF+RT) real folded potential and WS imaginary potential taken from Table III (solid lines). The far-side scattering cross sections are given by the same real folded OP but with different absorptive strengths W_V of the WS imaginary potential (dashed and dotted lines). Ak is the kth order Airy minimum.

in a future coupled reaction channel analysis of the elastic $^{16}O + ^{12}C$ scattering at low energies, to study the contribution of the elastic α-transfer process.

At 170 MeV, A1 and A2 are moved to $\theta_{c.m.} \approx 87°$ and $58°$, respectively. At 181 MeV, the locations of A1 and A2 are shifted to $\theta_{c.m.} \approx 79°$ and $52°$, respectively. However, the primary rainbow pattern associated with A1 is still somewhat obscured and not clearly seen in the elastic data measured at 170 and 181 MeV. Thus, the most optimal energy for the observation of the primary rainbow pattern in the $^{16}O + ^{12}C$ system is $E_{lab} = 200$ MeV as shown in Fig. 10, and the measured data are a very valuable probe of the strength and shape of the real OP for this system as discussed in Fig. 9.

With the incident energy increasing to above 200 MeV, the location of the Airy minima moves to the forward angles, as can be seen in the OM results for the elastic $^{16}O + ^{12}C$ scattering at $E_{lab} = 230$ to 608 MeV shown in Figs. 12 and 13. At 230 and 260 MeV, the first and second Airy minima are still visible in the measured data. The inspection of the far-side scattering cross section, especially that with a weaker absorptive strength of the imaginary OP, has shown that A1 is moved from $\theta_{c.m.} \approx 58°$ at 230 MeV to the c.m. angles of $48°$ and $44°$ at 260 and 281 MeV, respectively. Note that at
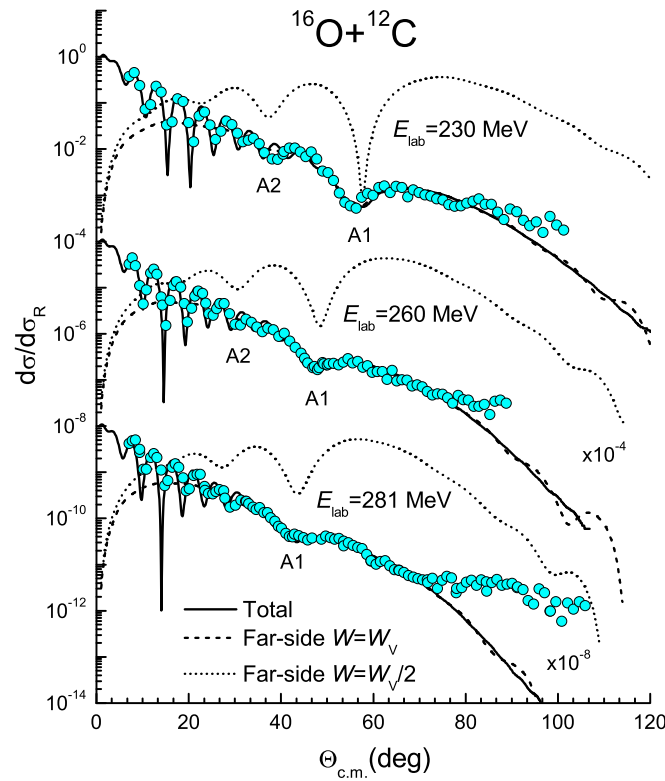
FIG. 12. The same as Fig. 11, but for the elastic $^{16}O + ^{12}C$ scattering data at $E_{lab} = 230$, 260, and 281 MeV [40,49,54].

FIG. 13. The same as Fig. 11, but for the elastic $^{16}O + ^{12}C$ scattering data at $E_{lab} = 300$, 330, and 608 MeV [54–56].

$E_{lab} = 281$ MeV the second Airy minimum A2 is moves into the diffractive part of the elastic cross section and is no longer visible in the measured data. A distinct feature of the elastic $^{16}O + ^{12}C$ scattering data at $E_{lab} = 281$, 300, and 330 MeV is the rise of the elastic cross section at large angles which is not caused by the Airy interference of the far-side trajectories [5,7]. Because the shallow minimum associated with such a rise in the elastic cross section at large angles seems also to be moving slowly to smaller scattering angles with the increasing energy, an alternative order of the Airy oscillation was suggested by Ogloblin *et al.* [49] to accommodate one more shallow Airy minimum in the $^{16}O + ^{12}C$ system at large angles. However, such an Airy oscillation pattern could not consistently fit in the Airy structure established for this same $^{16}O + ^{12}C$ system at lower energies or other refractive systems like $^{12}C + ^{12}C$ as discussed above in Fig. 6 or $^{16}O + ^{16}O$ [5,39]. An interesting scenario for the backward rise of the elastic $^{16}O + ^{12}C$ cross section at these energies has been suggested recently by Ohkubo *et al.* [61,62] as being due to a strong coupling of the elastic scattering to the inelastic 2^+ and 3^- excitations of the ^{12}C target. This important effect should be further checked by using other realistic choices of the OP and inelastic scattering potential for the $^{16}O + ^{12}C$ system. In particular, the elastic and inelastic folded potentials obtained in the present extended DFM that properly takes the RT into account should be a good choice for such a study. At the higher energies of $E_{lab} = 608$ and 1503 MeV the first Airy minimum A1 is well hidden in the forward angles, where only the Fraunhofer oscillation of the elastic cross section caused by the near-far interference [5,50]
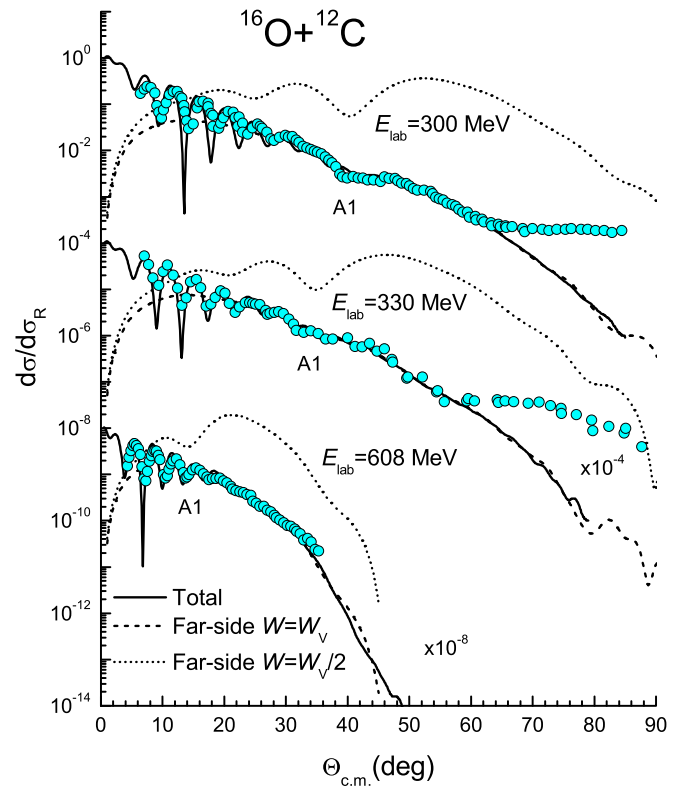
is visible in the measured data. Nevertheless, the large-angle exponential fall-off of the elastic cross section measured at these high energies is still dominated by the far-side scattering, and that has allowed us to determine the strength of the real folded (via N_R renormalization factor) quite accurately.

From the results of our detailed OM analysis of the elastic $^{16}O + ^{12}C$ scattering at energies up to 94 MeV/nucleon presented in Table III one can see that the extended DFM accounts quite well for the energy dependence of the real OP. At energies up to 21 MeV/nucleon, the best fit to the elastic $^{16}O + ^{12}C$ data has been achieved with the CDM3Y3 folded HF potential renormalized by the factor $N_R \approx 0.70$–0.75, while the best-fit renormalization factor of the folded HF+RT potential is $N_R \approx 0.95$–1.02. However, at the higher energies of 38 and 94 MeV/nucleon, the best-fit renormalization factor of the folded HF potential becomes $N_R \approx 0.66$–0.67. Given a realistic (mean-field based) energy dependence of the CDM3Yn interaction in terms of the $g(k(E, R))$ factor used in the extended DFM calculation (26)–(27), the best-fit renormalization factor of the real folded HF+RT potential remains close to unity at high energies ($N_R \approx 0.92$ and 1.02 at the energies of 38 and 94 MeV/nucleon, respectively). About the same trend was found with the best-fit N_R factors given by the real CDM3Y6 folded potential, which are about 3–5% larger than those obtained with the real CDM3Y3 folded potential. As discussed above in Sec. IV A, this effect is associated with a higher nuclear incompressibility given by the CDM3Y6 interaction that leads to a more repulsion in the real folded potential at small radii. To illustrate the local
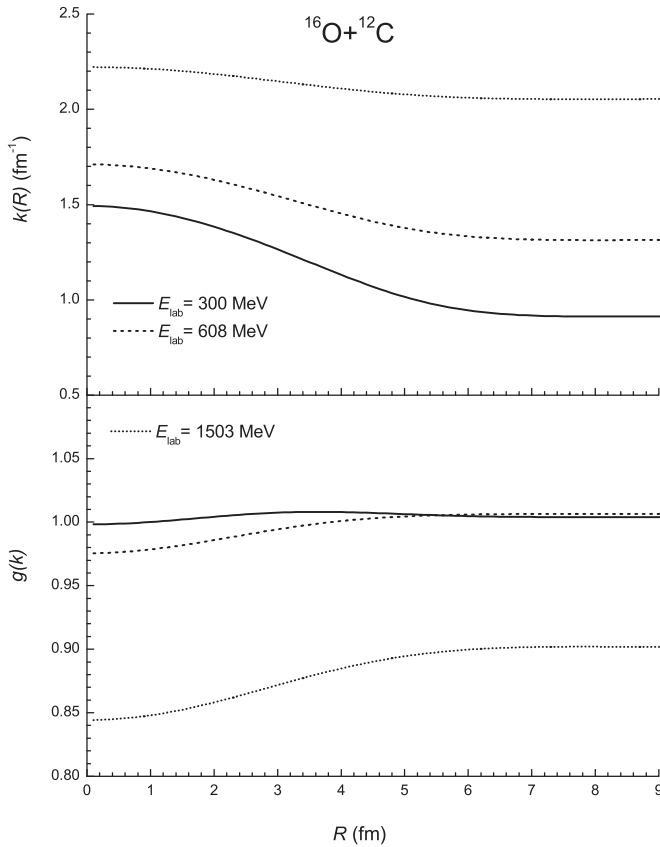
FIG. 14. Upper part: Local (average) nucleon momentum in the mean field based on the real folded $^{16}O+^{12}C$ potential $k(E,R) = K(E,R)/M$, where $K(E,R)$ is the relative-motion momentum (26). Lower part: Energy and radial dependence $g(k(E,R))$ of the CDM3Y3 interaction used in the folding calculation (27) of the $^{16}O+^{12}C$ potential, consistently interpolated from the explicit momentum dependence $g(k)$ of the nucleon OP shown in Fig. 4.

energy dependence $g(k(E,R))$ of the CDM3Y3 interaction used in the extended DFM calculation (27) of the $^{16}O+^{12}C$ potential, we have plotted the local (energy dependent) nucleon momentum $k(E,R)$ and the corresponding $g(k(E,R))$ factor in the upper and lower parts of Fig. 14, respectively. One can see that at low energies the real folded potential is deep at small distances R, so that the corresponding local relative-motion momentum $K(E,R)$ [see Eq. (26)] or the average nucleon momentum $k(E,R) = K(E,R)/M$ is significantly higher at small R compared to its asymptotic value at large R. The larger $K(E,R)$ value implies a quicker oscillation of the relative-motion wave function, and the deep real folded potential at low energies, as shown by Kondo *et al.* [51], usually generates the partial-wave radial functions having the numbers of nodes precisely as required by the Pauli principle when the dinuclear system is antisymmetrized. The local $g(k(E,R))$ factor (see lower part of Fig. 14) was consistently interpolated from the explicit momentum dependence $g(k)$ of the nucleon OP in NM shown in Fig. 4, and it represents, therefore, the mean-field based energy dependence of the CDM3Yn interaction used in the extended DFM calculation of the $^{16}O+^{12}C$ potential. At low energies ($E \lesssim 20$ MeV/nucleon) when $k(E,R) \lesssim$

1.6 fm^{-1}, the $g(k(E,R))$ factors remain close to unity. At the high energy of 94 MeV/nucleon, the $k(E,R)$ value is increased to above 2 fm^{-1} over the whole radial range (see upper part of Fig. 14) so that the corresponding $g(k(E,R))$ factor is reduced significantly (see lower part of Fig. 14). Thus, the consistent treatment of the mean-field based energy dependence of the CDM3Yn interaction via $g(k(E,R))$ factor helps to improve the predicting power of the real folded potential.

V. SUMMARY

The CDM3Y3 and CDM3Y6 density dependent versions of the M3Y-Paris interaction have been used in an extended HF study of symmetric NM, focusing on the rearrangement term of the single-nucleon potential that appears naturally when the Hugenholtz–van Hove theorem is taken into account in the calculation of the single-nucleon energy. Based on the exact expression of the RT of the density dependent single-nucleon potential given by the HvH theorem and the empirical energy dependence of the nucleon OP, a compact method has been proposed to account properly for the density and energy dependence of the RT of the nucleon OP in NM on the HF level.

Given an explicit contribution of the RT added to the density dependence of the CDM3Yn interaction and proper treatment of the momentum dependence of the nucleon mean-field potential in NM on the HF level, the double-folding model has been extended to take into account consistently the rearrangement effect in the DFM calculation of the nucleus-nucleus OP in the same mean-field manner. The contribution of the RT to the total nucleus-nucleus folded potential has been shown to be repulsive and particularly strong at small internuclear distances. This result is complimentary to the recent DFM calculation of the nucleus-nucleus OP using a G-matrix interaction that includes effectively the three-body force [63]. In fact, the microscopic origin of the RT was shown in the BHF study of NM [23,24] to be due to the higher-order diagram in the perturbative expansion of the mass operator and the contribution of the three-body force.

The present extension of the DFM is an important milestone that allows us to obtain the realistic shape and strength of the real folded OP at small internuclear distances, which match closely those implied by the detailed OM analysis of the elastic $^{12}C+^{12}C$ and $^{16}O+^{12}C$ scattering data measured at the refractive energies. The realistic treatment of the (mean-field based) energy dependence of the CDM3Yn interaction in the extended DFM calculation significantly improves the predicting power of the real folded potential, especially in the proper description of the Airy structure of the nuclear rainbow pattern observed in the elastic $^{12}C+^{12}C$ and $^{16}O+^{12}C$ scattering. All parameters of the modified density dependence of the CDM3Yn interaction that takes into account the correction by the RT and the mean-field based energy dependence are given in such details that the interested readers could easily include these parameters into their folding model calculation. The present development of the DFM for the nucleus-nucleus OP can be generalized and applied further in the folding model study of the inelastic nucleus-nucleus scattering [4], to reveal, in particular, the impact of the rearrangement effect caused by the nuclear excitation. This is the object of our further research.

ACKNOWLEDGMENTS

[1] G. R. Satchler and W. G. Love, Phys. Rep. **55**, 183 (1979).

[2] D. T. Khoa and W. von Oertzen, Phys. Lett. B **342**, 6 (1995).

[3] D. T. Khoa, G. R. Satchler, and W. von Oertzen, Phys. Rev. C **56**, 954 (1997).

[4] D. T. Khoa and G. R. Satchler, Nucl. Phys. A **668**, 3 (2000).

[5] D. T. Khoa, W. von Oertzen, H. G. Bohlen, and S. Ohkubo, J. Phys. G **34**, R111 (2007).

[6] H. Feshbach, *Theoretical Nuclear Physics*, Vol. II (Wiley, New York, 1992).

[7] M. E. Brandan and G. R. Satchler, Phys. Rep. **285**, 143 (1997).

[8] G. Bertsch, J. Borysowicz, H. McManus, and W. G. Love, Nucl. Phys. A **284**, 399 (1977).

[9] N. Anantaraman, H. Toki, and G. F. Bertsch, Nucl. Phys. A **398**, 269 (1983).

[10] A. M. Kobos, B. A. Brown, P. E. Hodgson, G. R. Satchler, and A. Budzanowski, Nucl. Phys. A **384**, 65 (1982).

[11] D. T. Khoa and W. von Oertzen, Phys. Lett. B **304**, 8 (1993).

[12] D. T. Khoa, G. R. Satchler, and W. von Oertzen, Phys. Rev. C **51**, 2069 (1995).

[13] G. E. Brown, Rev. Mod. Phys. **43**, 1 (1971).

[14] A. B. Migdal, *Theory of Finite Fermi Systems and Applications to Atomic Nuclei* (Interscience, New York, 1967).

[15] N. M. Hugenholtz and L. Van Hove, Physica **24**, 363 (1958).

[16] P. Czerski, A. De Pace, and A. Molinari, Phys. Rev. C **65**, 044317 (2002).

[17] D. T. Loan, B. M. Loc, and D. T. Khoa, Phys. Rev. C **92**, 034304 (2015).

[18] K. A. Brueckner and D. T. Goldman, Phys. Rev. **116**, 424 (1959).

[19] D. Vautherin and D. M. Brink, Phys. Rev. C **5**, 626 (1972).

[20] P. H. Heenen and M. R. Godefroid, Scholarpedia **7**, 10545 (2012).

[21] P. E. Hodgson, Rep. Prog. Phys. **38**, 847 (1975).

[22] D. T. Khoa, W. von Oertzen, and A. A. Ogloblin, Nucl. Phys. A **602**, 98 (1996).

[23] C. Mahaux, P. F. Bortignon, R. A. Broglia, and C. H. Dasso, Phys. Rep. **120**, 1 (1985).

[24] W. Zuo, I. Bombaci, and U. Lombardo, Phys. Rev. C **60**, 024605 (1999).

[25] A. Bohr and B. R. Mottelson, *Nuclear Structure*, Vol. I (W. A. Benjamin, New York, 1969), p. 237.

[26] R. L. Varner, W. J. Thompson, T. L. McAbee, E. J. Ludwig, and T. B. Clegg, Phys. Rep. **201**, 57 (1991).

[27] S. Hama, B. C. Clark, E. D. Cooper, H. S. Sherif, and R. L. Mercer, Phys. Rev. C **41**, 2737 (1990).

[28] C. Mahaux and R. Sartor, *Advances in Nuclear Physics*, edited by J. W. Negele and Erich Vogt, Vol. 20 (Kluwer Academic Publishers, New York, 1991), p. 1.

[29] D. T. Khoa, W. von Oertzen, and H. G. Bohlen, Phys. Rev. C **49**, 1652 (1994).

[30] D. T. Khoa, Phys. Rev. C **63**, 034007 (2001).

[31] S. H. Fricke, M. E. Brandan, and K. W. McVoy, Phys. Rev. C **38**, 682 (1988).

[32] M. E. Brandan, M. S. Hussein, K. W. McVoy, and G. R. Satchler, *Comments on Nuclear and Particle Physics*, Vol. 22 (Gordon and Breach, New York, 1996), p. 77.

[33] D. M. Brink and N. Takigawa, Nucl. Phys. A **279**, 159 (1977).

[34] N. Rowley, H. Doubre, and C. Marty, Phys. Lett. B **69**, 147 (1977).

[35] K. W. McVoy and M. E. Brandan, Nucl. Phys. A **542**, 295 (1992).

[36] R. M. Wieland, R. G. Stokstad, G. R. Satchler, and L. D. Rickertsen, Phys. Rev. Lett. **37**, 1458 (1976).

[37] R. G. Stokstad, R. M. Wieland, G. R. Satchler, C. B. Fulmer, D. C. Hensley, S. Raman, L. D. Rickertsen, A. H. Snell, and P. H. Stelson, Phys. Rev. C **20**, 655 (1979).

[38] M. E. Brandan and G. R. Satchler, Nucl. Phys. A **487**, 477 (1988).

[39] D. T. Khoa, W. von Oertzen, H. G. Bohlen, and F. Nuoffer, Nucl. Phys. A **672**, 387 (2000).

[40] A. A. Ogloblin, Y. A. Glukhov, V. Trzaska, A. S. Demyanova, S. A. Goncharov, R. Julin, S. V. Klebnikov, M. Mutterer, M. V. Rozhkov, V. P. Rudakov, G. P. Tiorin, D. T. Khoa, and G. R. Satchler, Phys. Rev. C **62**, 044601 (2000).

[41] J. E. Poling, E. Norbeck, and R. R. Carlson, Phys. Rev. C **13**, 648 (1976).

[42] J. Raynal, *Computing as a Language of Physics* (IAEA, Vienna, 1972), p. 75; coupled-channel code ECIS97 (unpublished).

[43] J. Y. Hostachy, M. Buenerd, J. Chauvin, D. Lebrun, Ph. Martin, J. C. Lugol, L. Papineau, P. Roussel, N. Alamanos, J. Arvieux, and C. Cerruti, Nucl. Phys. A **490**, 441 (1988).

[44] S. Kubono, K. Morita, M. H. Tanaka, M. Sugitani, H. Utsunomiya, H. Yonehara, M. K. Tanaka, S. Shimoura, E. Takada, M. Fukuda, and K. Takimoto, Phys. Lett. B **127**, 19 (1983).

[45] H. G. Bohlen, X. S. Chen, J. G. Cramer, P. Fröbrich, B. Gebauer, H. Lettau, A. Miczaika, W. von Oertzen, R. Ulrich, and Th. Wilpert, Z. Phys. A **322**, 241 (1985).

[46] A. S. Demyanova, H. G. Bohlen, A. N. Danilov, S. A. Goncharov, S. V. Khlebnikov, V. A. Maslov, Yu. E. Penionzkevich, Yu. G. Sobolev, W. Trzaska, G. P. Tyurin, and A. A. Ogloblin, Nucl. Phys. A **834**, 473c (2010).

[47] A. J. Cole, W. D. M. Rae, M. E. Brandan, A. Dacal, B. G. Harvey, R. Legrain, M. J. Murphy, and R. G. Stokstad, Phys. Rev. Lett. **47**, 1705 (1981).

[48] M. Buenerd, A. Lounis, J. Chauvin, D. Lebrun, P. Martin, G. Duhamel, J. C. Gondrand, and P. De Saintignon, Nucl. Phys. A **424**, 313 (1984).

[49] A. A. Ogloblin, S. A. Goncharov, Yu. A. Glukhov, A. S. Demyanova, M. V. Rozhkov, V. P. Rudakov, and W. H. Trzaska, Phys. At. Nucl. **66**, 1478 (2003).

[50] R. C. Fuller, Phys. Rev. C **12**, 1561 (1975).

[51] Y. Kondō, M. E. Brandan, and G. R. Satchler, Nucl. Phys. A **637**, 175 (1998).

[52] M. E. Brandan and G. R. Satchler, Phys. Lett. B **256**, 311 (1991).

[53] A. A. Ogloblin, D. T. Khoa, Y. Kondō, Yu. A. Glukhov, A. S. Demyanova, M. V. Rozhkov, G. R. Satchler, and S. A. Goncharov, Phys. Rev. C **57**, 1797 (1998).

[54] A. S. Demyanova *et al.*, IAEA Database EXFOR, http://www-nds.iaea.org/exfor/

[55] M. E. Brandan, A. Menchaca-Rocha, L. Trache, H. L. Clark, A. Azhari, C. A. Gagliardi, Y.-W. Lui, R. E. Tribble, R. L. Varner, J. R. Beene, and G. R. Satchler, Nucl. Phys. A **688**, 659 (2001).

[56] M. E. Brandan, A. Menchaca-Rocha, M. Buenerd, J. Chauvin, P. DeSaintignon, G. Duhamel, D. Lebrun, P. Martin, G. Perrin, and J. Y. Hostachy, Phys. Rev. C **34**, 1484 (1986).

[57] P. Roussel-Chomaz, N. Alamanos, F. Auger, J. Barrette, B. Berthier, B. Fernandez, and L. Papineau, Nucl. Phys. A **477**, 345 (1988).

[58] S. Szilner, W. von Oertzen, Z. Basrak, F. Haas, and M. Milin, Eur. Phys. J. A **13**, 273 (2002).

[59] M. C. Morais and R. Lichtenthäler, Nucl. Phys. A **857**, 1 (2011).

[60] A. T. Rudchik *et al.*, Eur. Phys. J. A **44**, 221 (2010).

[61] S. Ohkubo and Y. Hirabayashi, Phys. Rev. C **89**, 051601(R) (2014).

[62] S. Ohkubo, Y. Hirabayashi, A. A. Ogloblin, Yu. A. Gloukhov, A. S. Demyanova, and W. H. Trzaska, Phys. Rev. C **90**, 064617 (2014).

[63] K. Minomo, M. Toyokawa, M. Kohno, and M. Yahiro, Phys. Rev. C **90**, 051601(R) (2014).